A Passive On-line Defect Detection Method for Wire and Arc Additive Manufacturing Based on Infrared Thermography

Xi Chen*, Haiou Zhang*, Jiannan Hu*, Yu Xiao*

* School of mechanical science and engineering, Huazhong University of Science and Technology, Wuhan 430074, PR China

Abstract

According to the additive manufacturing process, this paper comes up with a passive infrared thermography non-destructive testing method based on the stack temperature field and pixel width curve. The temperature field of the arc-melting layer is collected in real-time, and the multi-frame temperature data stream is stacked for maximum value, and the region where the maximum value is greater than 800 °C is intercepted to obtain the current molten layer profile. The AlexNet model is used to classify the profile of molten layers, such as normal, deviation, flow and hump. Determine whether the current layer has a shape defect based on the model and the pixel width curve and the processing such as milling and repair welding will be taken in time. This method detects in real-time during the manufacturing process which will cause irreversible losses, and the current layer detection information is also the basis for adjusting the processing parameters of the next layer and realizes the closed-loop feedback of the additive manufacturing process.

Introduction

The arc deposition additive manufacturing technology has the advantages of formable complex shapes, high deposition efficiency, and low cost[11][14]. At the same time, it is also a multi-physics coupling process, which is affected by factors such as welding current, voltage, trajectory, walking speed, wire feeding speed, and wire material purity. The molten layer may occur defects such as hump, flow, and deviation, which ultimately affect the size and quality of the formed part. The current layer should be detected in real-time, and the defect is milled or repaired according to the detection result, and the process parameters are fed back to the system as the basis for the next layer adjustment to ensure the quality of the additive product. Limited by the detection conditions, in the actual production process, the parts are detected after the overall forming, such as X-ray, ultrasonic, eddy current, infiltration, etc., however, these methods have many limitations, such as radiation safety hazards, the need for couplant, contact measurement, etc., resulting in the inability to detect online in real-time[12][13].

Arc deposition additive manufacturing accompany high-temperature so that the infrared thermography has a wide application in process monitoring[1]. The infrared thermal image detection technology has the advantages of fast response, large detection range, intuitive detection results, non-contact, etc., and can be preferably used for online defect detection in the arc deposition process[2][3][4][5]. According to whether an external heating source is needed, the infrared thermal image detection technology is divided into active and passive, and passive refers to the means of detecting only the process of heat exchange between the measured object and the surrounding environment. The active method is to inject heat into the measured object in a confined space, so that the target has a thermal imbalance state at the defect, and analyzes the law of the heat transfer process, thereby realizing detection.

V.P. Vavilov et al. (2015) developed a one-sided thermal non-destructive testing based on multiplying front-surface temperature evolution by n^{th} power of time. This is an active detection method by injecting a steady heat flow into a sample and observe the change curve of $T \cdot \tau^{0.4}(℃ \cdot S)$ to identify the difference between defect and normal area. This method can identify defects well but is not suitable for industrial field measurement[6].

Sadek C. Absi Alfaro et al. (2015) developed a methodology for hump defect based on temperature gradient analysis in real-time. They established the relationship between sudden changes in temperature distribution and defects, and considered that thermal imaging monitoring of welding defects could be used for online detection and control of welding process discontinuities[7].

When the defect detection is based on temperature field analysis, the selection of characteristic parameters is critical, which is closely related to the materials, welding mode, substrate size and so on. Choosing a suitable characteristic parameter to maximize the difference between the defect area and the normal area is a difficult problem in current research, which affects the universality of the system. In this paper, a passive infrared thermal image detection method is proposed. The profile is extracted by stacking the temperature field. The defect identification of hump, flow and deviation are performed according to the profile information. The training is performed by AlexNet model, and the online real-time detection of defects is finally realized.

Experimental procedure

Figure 1 shows a schematic diagram of the experimental set-up and the process of on-line defect detecting, as shown in the left half, the experiments are based on a LORCH welder under pulse model and a Yaskawa robot, which are both controlled by an industrial computer[10]. The surface temperature field was collected by a MAG32 thermal imager, with a pixel of 384*288, a minimum phase element size of 17μm, a temperature range of -20℃-1600℃, and a frame rate of 50HZ. The thermal imager and the substrate are fixed together, and the welding torch walks different tracks to form the weld bead. It is worth mentioning that in the whole welding process, because the relative position of the thermal imager and the substrate is unchanged,

therefore, in the multi-frame bead data collected, the position of each point on the bead is always constant.

By using different process parameters, samples with various defects are generated to prepare for the training classification. Without special instructions, the material of sample and welding wire are all carbon steel, with the rated voltage of 27.8V and the rated current of 238A, the protection gas of argon with 10% CO_2, the gas flow rate of 20L/min, and the wire feeding speed of 7.5m/min.

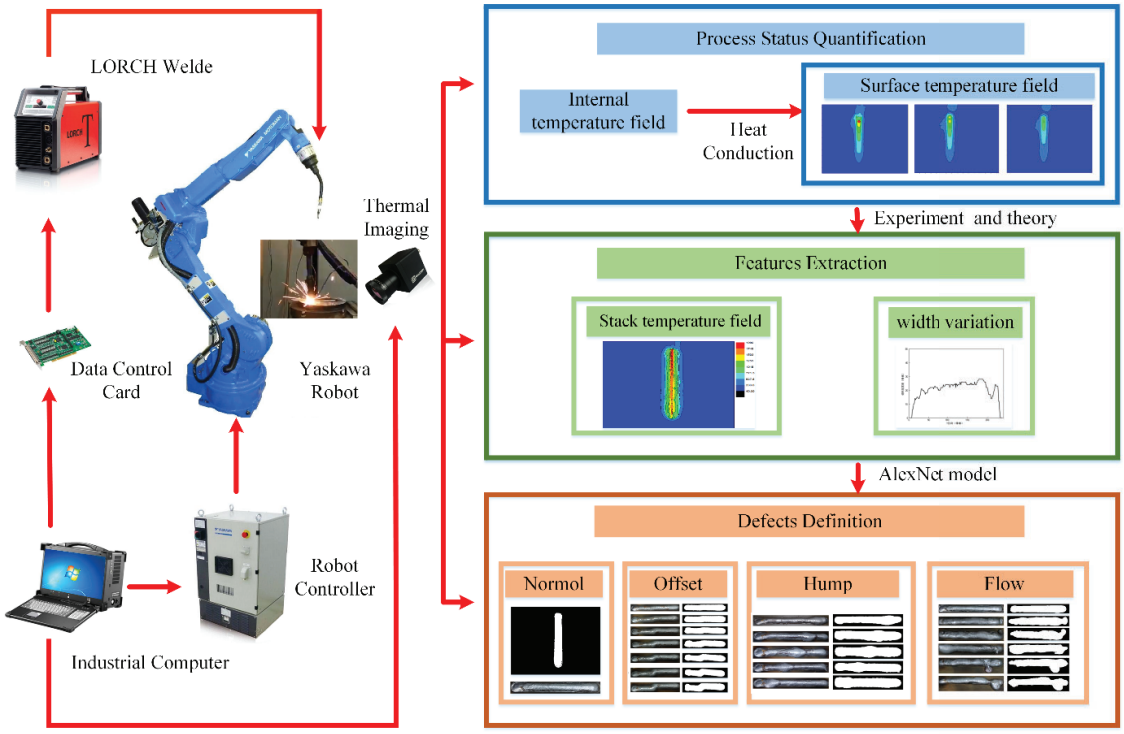

Figure 1. The experimental set-up and the process of the on-line defect detecting

Normal weld bead

In the process, to produce a normal weld bead, the wire feeding speed, the clamping mechanism, the welding trajectory are stable, the interlayer temperature is kept below 150 ° C, the substrate and the weld bead surface are clean, and the deposition velocity is 300 mm / min. Real-time temperature field of weld bead surface was collected by thermal imager after arc extinction, and is shown in figure 2 at 0s, 2s, 5s, 10s.

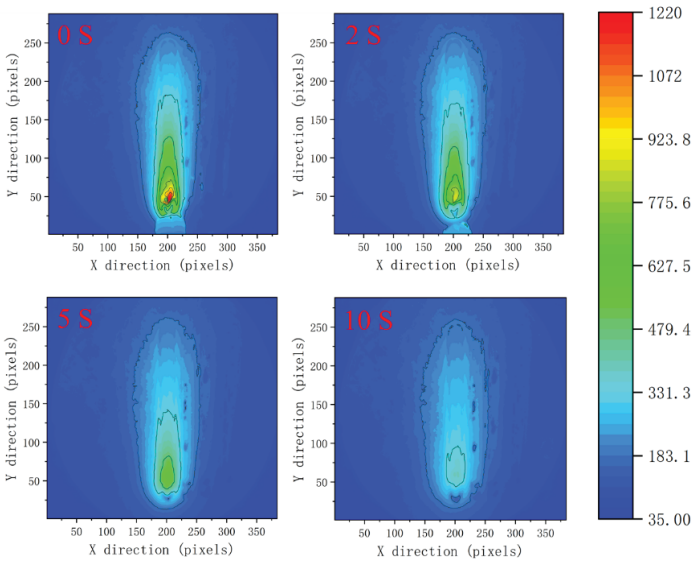

Figure 2. The temperature field of normal weld bead surface in the process of cooling

Weld bead deviation defect

In the actual production process, the deviation of the welding gun, the instability of the clamping mechanism, and the wrong trajectory of the robot will all result in the weld bead deviation. In this paper, the weld bead with different deviation degrees from 1mm to 7mmm is obtained by setting different deposition trajectories, and the deposition velocity is 300mm/min. Real-time temperature field of weld bead surface was collected by thermal imager after arc extinction, and is shown in figure 3 at 0s, 2s, 5s, 10s.

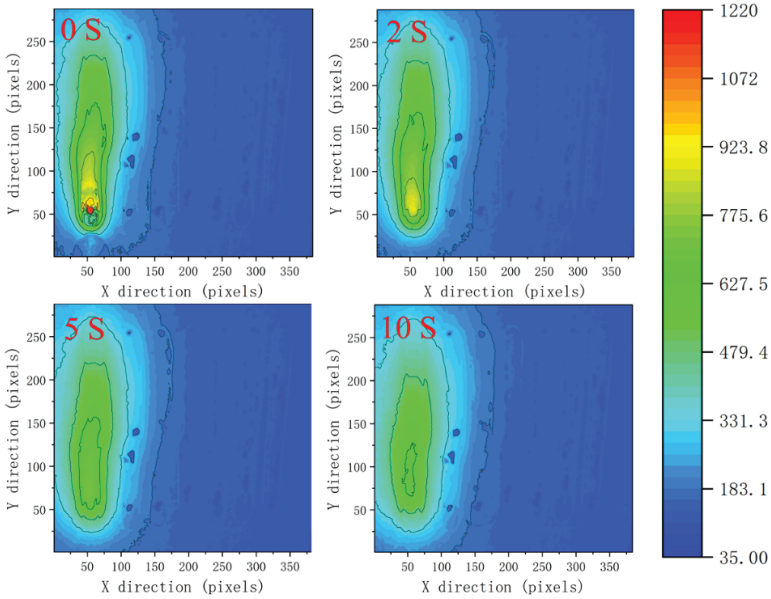

Figure 3. The temperature field of deviation weld bead surface in the process of cooling

Weld bead hump defect

In the actual production process, the sudden uneven deposition rate and the unsmooth wire feed will result in the hump defect. In this paper, the weld bead with hump defect is obtained by pausing 2S at different deposition, and the deposition velocity is 300mm/min. Real-time temperature field of weld bead surface was collected by thermal imager after arc extinction, and is shown in figure 4 at 0s, 2s, 5s, 10s

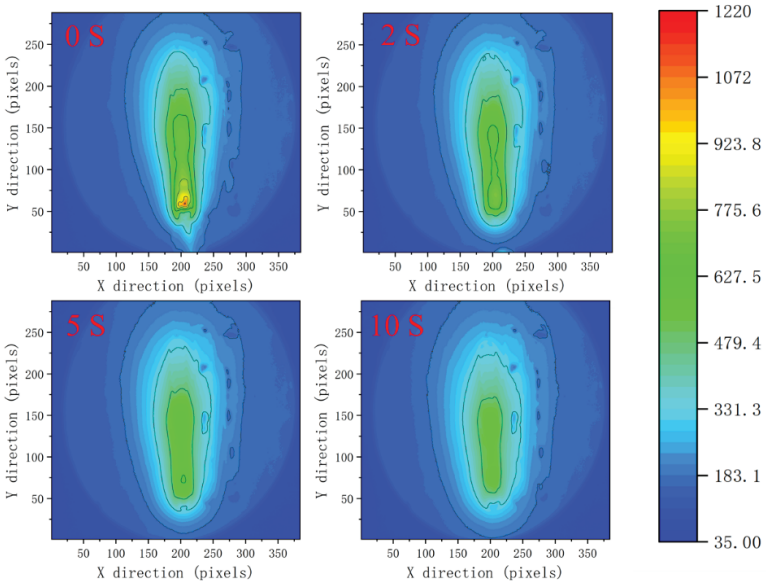

Figure 4. The temperature field of the hump weld bead surface in the process of cooling

Weld bead flow defect

In the actual production process, usually, the flow defect occurs at high deposition layer, because of the sudden uneven deposition rate and the high temperature of the last layer. As a result, the area of the current deposition layer is larger than the area that can be stacked. In this paper, the deposition velocity of 300mm/min is adopted to stack five layers, and the deposition velocity is reduced to 250mm/min to imitate the flow defect of the deposition layer in actual production. Real-time temperature field of weld bead surface was collected by thermal imager after arc extinction, and is shown in figure 5 at 0s, 2s, 5s, 10s

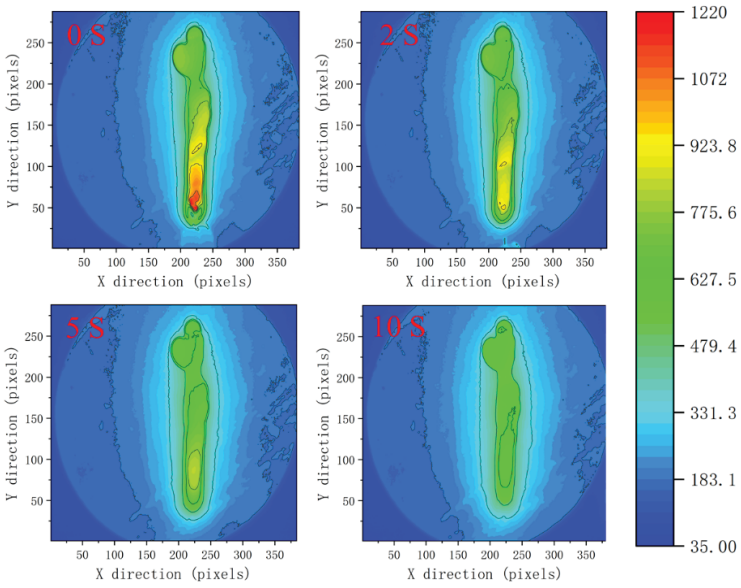

Figure 5. The temperature field of flow weld bead surface in the process of cooling

In order to better illustrate the welding trajectory, the schematic diagram is shown in figure 6, and the black line, the red circle, the blue circle, and the yellow circle represents the trajectory of the torch, the arcing point, the arc blowout point, and the pause point.

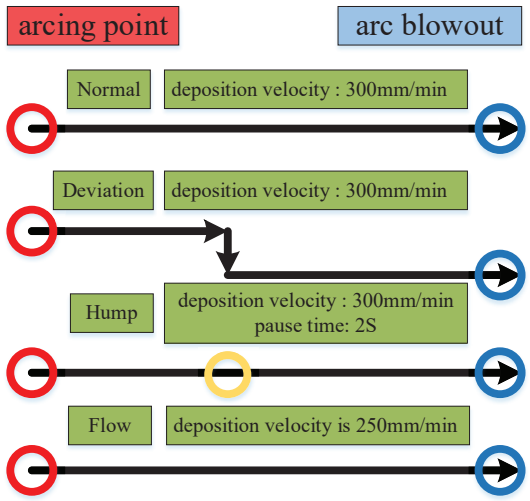

Figure 6. Schematic diagram of sample trajectory planning

Infrared image of the deposition layer: analysis and results

1. Stacking of temperature fields

As shown in section 2, in the surface temperature field acquired in real-time, the contour of the molten layer is blurred and varies significantly with temperature. Due to the heat

dissipation effect, the temperature difference between the head and the tail of the weld bead is large, and the temperature gradient between the substrate and the weld bead is small so that the contour of the molten layer cannot be extracted well.

In this paper, the image stacking method is used to stack the multi-frame temperature data, and finally obtain the highest temperature of each pixel. Taking the point A with coordinates (x, y) as an example, (each frame data of the thermal imager contains the real-time temperature of 384*288 pixels, with the lower-left corner as the point (1, 1) , the value of 'x' ranges from 1 to 384, and the value of 'y' ranges from 1 to 288). Assume that n frames data are collected during the welding process, and the real-time temperature of point A is T_n. The first frame temperature T_1 and the second frame temperature T_2 are compared, and the larger one is defined as T_{max}=max $\{T_1, T_2\}$, and the third frame temperature T_3 and T_{max} are compared, and the larger value is redefined as T_{max}. = max $\{ T_{max}, T_3\}$= max $\{ \max \{ T_1, T_2\}, T_3\}$, so that the loop is repeated until the last frame of data is compared, and T_{max}=max $\{T_{max}, T_n\}$ is obtained, thereby achieving temperature stacking. As can be seen from figure 7, the temperature gradient between the stacked substrate and the weld bead becomes larger, and the weld bead profile becomes more conspicuous.

Finally, the stack temperature field is subjected to threshold segmentation processing to obtain a weld bead profile, and a reasonable temperature threshold T_D is set. The stack temperature T_{max} is compared with T_D, and the value greater than or equal to T_D is re-assigned to 0, the value less than T_D is re-assigned to 1. Each pixel is compared to T_D, and the pixel with a value of 0 is drawn as white, and the pixel with a value of 1 is drawn as black. The weld bead profile is finally obtained.

The experiments in this paper are all based on carbon steel materials, by comparing and analyzing the temperature field of multiple experiments, it is found that the temperature of the molten layer is more than 800 ° C, so T_D is set to 800 ° C, the region equal to or higher than T_D is extracted to separate the weld bead and substrate and obtain profile.

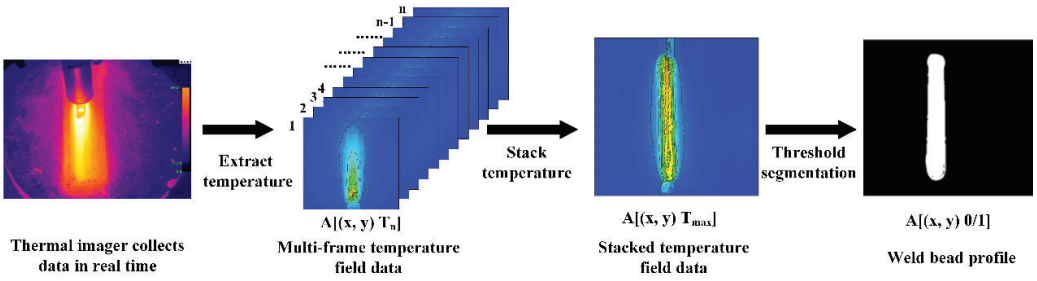

Figure 7. Schematic diagram of temperature stacking algorithm

The temperature field information of the three kinds of defects in Chapter 2 is stacked to obtain the weld bead profile, as shown in figure 8. These profile images will be used as the training and test set for the AlexNet model in Chapter 4 to achieve the online detection of defects. Figure 9 is a natural image of the weld bead. The comparison of figure 8 and figure 9 verifies the reliability of the temperature field stacking method.

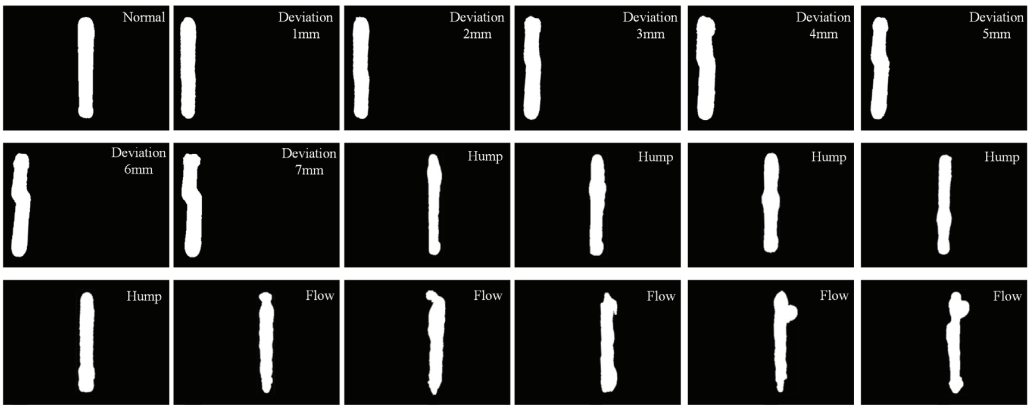

Figure 8. The weld bead profile with different defects

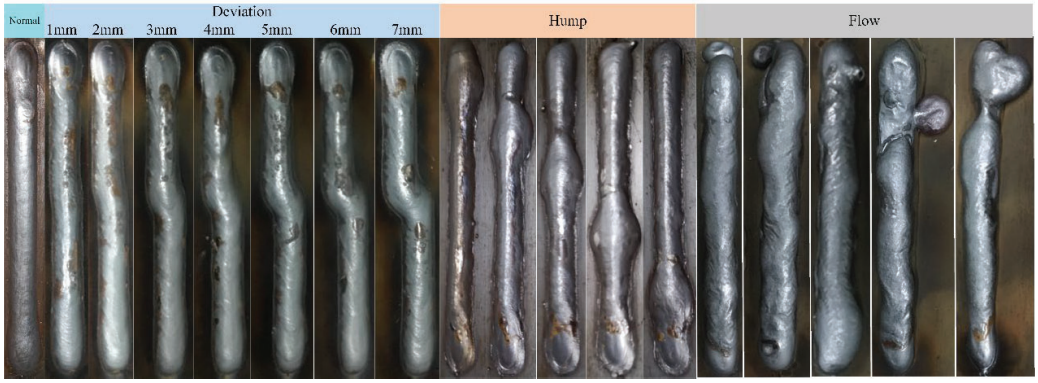

Figure 9. The natural image of the weld bead with different defects

2. Information extraction of weld bead width

Through the analysis of the weld bead profile information with hump defects, flow defects and offset defects, it is found that when similar morphological defects occur, the weld bead width will change significantly. It is possible to judge whether or not a defect occurs depending on the curve of the bead width, and it is not necessary to obtain an accurate value of the bead width.

As shown in figure 10, According to the image information divided by the threshold in Section 3.1, scan each line from bottom to top, and search for the first and last point A (x1, y), B(x1, y) from left to right. The pixel width is x2-x1, which is sequentially scanned to obtain a curve of the pixel width from the arcing point to the arcing blowout point.

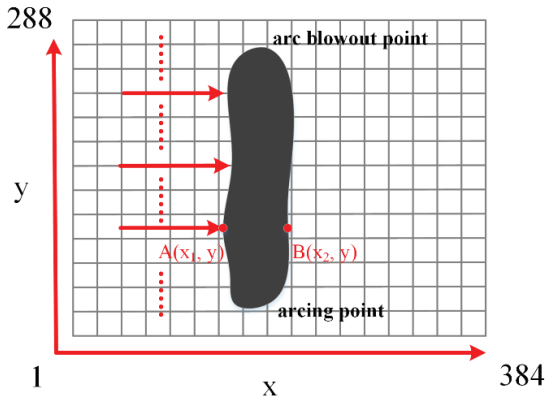

Figure 10. Schematic diagram of weld bead pixel width extraction

According to the above algorithm, the curve of the pixel width of the normal weld bead, the weld bead with different deviation degrees, the hump weld bead at different positions, and the flow bead of different degrees are shown in figure 11. The width information of the arcing point and the arcing blowout point are not used as the judging area, the normal weld bead width curve is smooth, and the pixel width does not change much. When the offset is 1mm, there is no large difference in the width curve. Other defect weld beads show obvious sudden or irregular changes in the width curve.

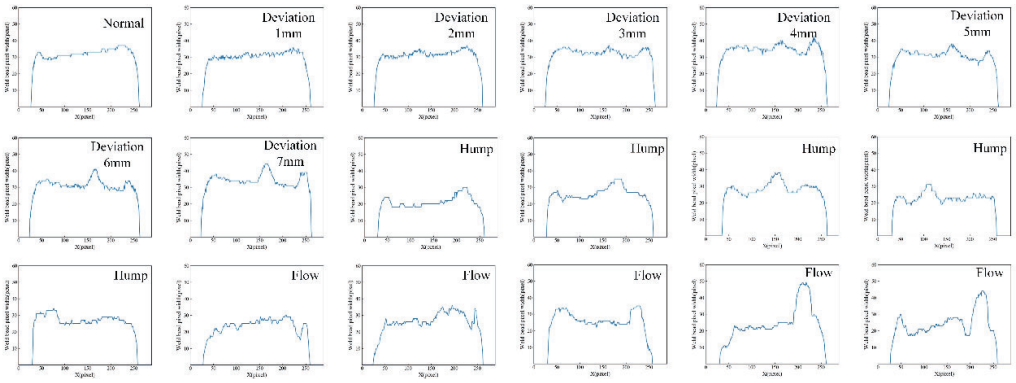

Figure 11. The weld bead pixel width curve

Therefore, the curve of the weld bead width can be used as the basis for judging the defects of the weld bead. When the width is significantly changed, the defect of the current layer can be judged, and the defect information is immediately fed back to the system for milling and repair welding. At the same time as the basis for the adjustment of the second layer of process parameters.

In this paper, a composite detection method is proposed that compensates for the limitations of a single detection method. The detection method based on the pixel width curve has relatively high accuracy, but the arcing point and the arc blowout point are not considered. The detection method based on the AlexNet model takes the entire bead profile as the object of discrimination, but the accuracy is affected by the sample and test set, and the generalization ability is weak. In this paper, the two methods are used to synchronously detect weld bead contour defects and enhance the detection rate of defects.

Weld bead profile defect identification based on AlexNet model

1. AlexNet model

In this paper, the AlexNet model is used to classify the normal weld bead, weld bead deviation defect, weld bead hump defect, and weld bead flow defect based on the profile images. In the AlexNet model, ReLU is used as an activation function of CNN to successfully solve the gradient dispersion problem[8]. Dropout is used to randomly ignore a subset of neurons at the fully connected layer to avoid over-fitting the model during training. The maximum pooling (step size is smaller than the convolution kernel) is used to instead of the average pooling, which avoids the average pooling blur effect and improves the feature richness. The LRN layer (Local Response Normalization) is proposed to create a competition mechanism for the activity of local neurons so that the larger response is magnified, and the other neurons with smaller feedback are suppressed, and the enhancement is enhanced. The generalization ability of the model. The schematic diagram of the AlexNet model is shown in figure 12[9].

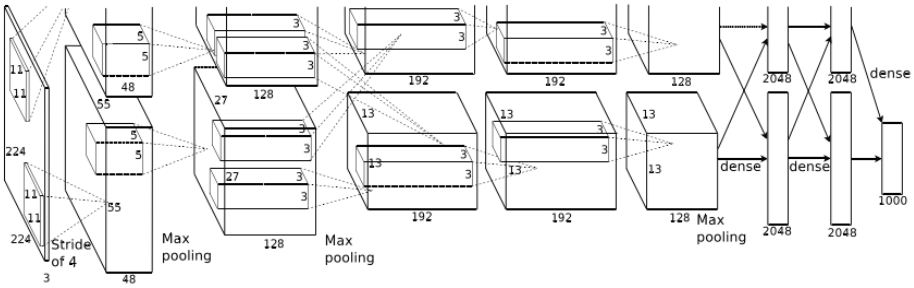

Figure 12. Schematic diagram of AlexNet model

The AlexNet model uses an 8-layer neural network, including 630 million links, 60 million parameters and 65 neurons, 5 convolutional layers and 3 fully connected layers (3 convolutional layers followed by a maximum pooling layer). The input to the model is a 56×224 size bead profile picture. Randomly intercepting the 56×56 size area (and the horizontally flipped image) is equivalent to an increase of 336 times the amount of data, which increases the generalization ability of the model.

In the first convolutional layer conv1, AlexNet uses a 96×11×11 convolution kernel with a convolution kernel of 4 steps. The second convolution kernel is 5 × 5, and the remaining convolution kernels are 3 × 3. The activation function uses ReLU to prevent the gradient from disappearing. The last fully-connected layer fc8 is connected by all the neurons of the previous fc7, and outputs a k-dimensional vector, where k is the number of categories of the classification. In this paper, the infrared profile of the weld layer includes four categories: normal, hump, flow and deviation, so k takes 4. The schematic diagram of the AlexNet model structure is shown in figure 13.

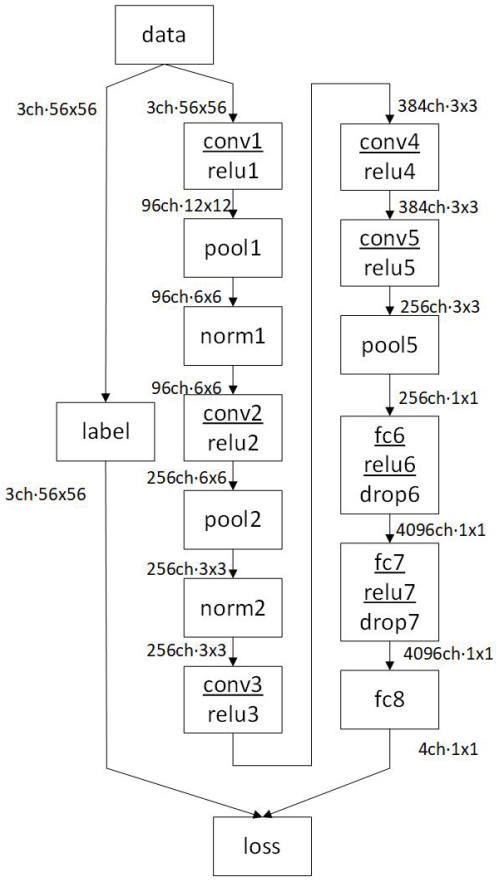

Figure 13. Schematic diagram of AlexNet model structure

2. Data set construction and training

In this paper, the number of samples is increased by extracting the stack results of different continuous frames of temperature data. The weld bead profile data for each category in this paper is shown in Table 1. The training set and verification set ratio are divided according to about 3:1.

Table 1. Summary of four categories of profile data sets

category	Number of training sets	Number of test sets
normal	1458	368
deviation	1040	331
hump	702	226
flow	1163	343

The Caffe deep learning framework was used to build the AlexNet model (graphics card: GTX1060), the initial learning rate is 0.001, the learning rate strategy is selected, and the momentum is 0.9. 100 pieces of training are taking after 500 iterations. Due to the small number of samples, it is easy to produce over-fitting, so that some methods are used to increases the generalization ability of the model and reduces the model overfitting.

(1) The L2 regularization method, where L2 is taken as 0.00001.
(2) The Dropout layer is set before the last average pooling layer, and the probability of random inactivation of neurons is 0.5.
(3) Randomly crop the 200×56 size image and resize it to 224×56. Data enhancement is achieved by a random horizontal and vertical flip of 5 degrees.

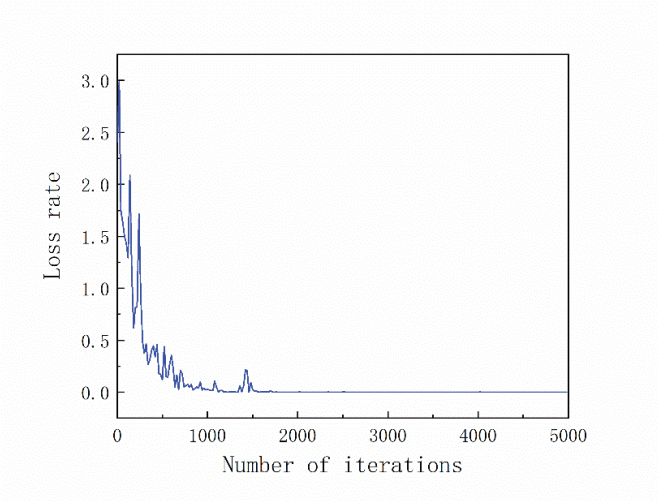

Figure 14. The loss rate in the network training process

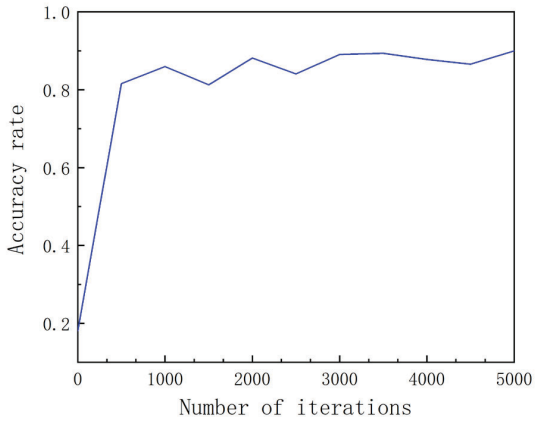

Figure 15. The accuracy rate in the network training process

The accuracy rate and the loss rate in the network training process are shown in figure 14, 14. After 2000 iterations, the loss rate reaches 3.8e-4, and the accuracy rate reaches 91% after 5,000 iterations. The bead profile recognition classification based on the AlexNet model only takes 1.35ms, which can meet the requirements of online real-time detection. The offset, hump, and flow are quickly detected and fed back, which facilitates the optimization of the process parameters of the next layer and ensures the quality of the additive products.

Conclusion

In order to detect the defects of weld bead shape, such as deviation, hump, flow, this paper

come up with a composite method based on the stack temperature field and the width curve. Different from the traditional infrared nondestructive testing, this method does not need an external heat source, which makes online testing possible.

The surface temperature field is stacked to get the weld bead profile and analyzed by the computer in real-time. The stack of temperature field can solve the problem of unclear contour boundary caused by heat dissipation of substrate, After the temperature field is stacked, all pixel points whose temperature used to be above the threshold are extracted to form the weld bead contour.

The AlexNet model is used to distinguish the normal weld bead and defect weld bead, which only takes 1.35ms. Because the accuracy of the model could not reach 100%, a defect detection method based on the pixel width curve of contour was proposed. Through the compound discrimination of the two methods, the identification rate of the melt layer defect was improved, and the defect information was fed back to the system for repair welding and milling, so as to realize the online detection of additive manufacturing defect. By strictly controlling the quality of each layer, unusable waste products are avoided after forming.

Through research, we believe that the infrared thermography has broad application prospects in nondestructive testing. By studying the influence of defects on the surface temperature field of the molten layer, the appropriate features can be extracted to identify and classify defects.

References:

[1] Hu C, Chen X Z. A Review and Preliminary Experiment on Application of Infrared Thermography in Welding[C]//International Conference on Robotic Welding, Intelligence and Automation. Springer, Cham, 2014: 351-359.

[2] Chen W, Chin B A. Monitoring joint penetration using infrared sensing techniques[J]. Welding Journal, 1990, 69(4): 181s-185s.

[3] Banerjee P, Govardhan S, Wikle H C, et al. Infrared sensing for on-line weld geometry monitoring and control[J]. Journal of Engineering for Industry, 1995, 117(3): 323-330.

[4] Menaka M, Vasudevan M, Venkatraman B, et al. Estimating bead width and depth of penetration during welding by infrared thermal imaging[J]. Insight-Non-Destructive Testing and Condition Monitoring, 2005, 47(9): 564-568.

[5] Ghanty P, Vasudevan M, Mukherjee D P, et al. Artificial neural network approach for estimating weld bead width and depth of penetration from infrared thermal image of weld pool[J]. Science and Technology of Welding and Joining, 2008, 13(4): 395-401.

[6] Vavilov V P , Pawar S S . A novel approach for one-sided thermal nondestructive testing of composites by using infrared thermography[J]. Polymer Testing, 2015, 44:224-233.

[7] Alfaro S C A , Vargas, José Alfredo Ruiz, de Carvalho, Guilherme Caribé, et al. Characterization of “Humping” in the GTA welding process using infrared images[J]. Journal of Materials Processing Technology, 2015, 223:216-224.

[8] Krizhevsky A, Sutskever I, Hinton G E. Imagenet classification with deep convolutional

neural networks[C]//Advances in neural information processing systems. 2012: 1097-1105.
[9] Tuama A, Comby F, Chaumont M. Camera model identification with the use of deep convolutional neural networks[C]//2016 IEEE International workshop on information forensics and security (WIFS). IEEE, 2016: 1-6.
[10] Tang S, Wang G, Zhang H, et al. An online surface defects detection system for AWAM based on deep learning[J]. Proceedings of the 28th Solid Freeform Fabrication (SFF) symposium, Austin (Texas), 7-9 august, 2017.
[11] Karunakaran K P, Suryakumar S, Pushpa V, et al. Low cost integration of additive and subtractive processes for hybrid layered manufacturing[J]. Robotics and Computer-Integrated Manufacturing, 2010, 26(5):490-499.
[12] Energetics Inc. for National Institute of Standards and Technology, Measurement science roadmap for metal-based additive manufacturing, May-2013.
[13] D. L. Bourell, M. C. Leu, and D. W. Rosen, Roadmap for additive manufacturing: identifying the future of freeform processing, Univ. Tex. Austin, 2009.
[14] Hofmann D C, Roberts S, Otis R, et al. Developing Gradient Metal Alloys through Radial Deposition Additive Manufacturing[J]. Sci Rep, 2014, 4(4):5357.